THE ASTROPHYSICAL JOURNAL, 434:468–478, 1994 October 20

THE X-RAY SPECTRA OF BLAZARS OBSERVED WITH *EXOSAT*

RITA M. SAMBRUNA[1]
SISSA/ISAS, Strada Costiera 11, 34014 Trieste, Italy; rita@tsmil9.sissa.it
PAUL BARR
ISO Observatory, European Space Agency, ESTEC, Postbus 229, 2200 AG Noordwijk, The Netherlands
PAOLO GIOMMI
ESA/ESRIN, via Galileo Galilei, C.P. 64, 00044 Frascati, Italy
LAURA MARASCHI
Dipartimento di Fisica, via Dodecaneso 33, 16146 Genova, Italy
GIANPIERO TAGLIAFERRI
Osservatorio Astronomico di Brera, via Brera 28, I-20121 Milano, Italy
AND
ALDO TREVES
SISSA/ISAS, Strada Costiera 11, 34014 Trieste, Italy
Received 1993 May 7; accepted 1994 April 26

ABSTRACT

A systematic analysis of the X-ray spectra (0.1–10 keV) of all blazars observed with *EXOSAT* is presented. The objects include 16 X-ray–selected BL Lac objects (XBLs), five radio-selected BL Lac objects (RBLs), and five highly polarized quasars (HPQs). Comparing the results of single–power-law fits for the different classes, we find that XBLs have steeper X-ray spectra than HPQs (average photon indices $\langle\Gamma\rangle \sim 2.20^{+0.17}_{-0.15}$ and $1.62^{+0.11}_{-0.24}$, respectively). The X-ray luminosities of XBLs and RBLs are similar, while HPQs tend to be somewhat more luminous. For the three groups, a correlation between the average medium-energy luminosity and the average spectral index is found, in the sense that sources of higher luminosity have flatter spectra. For repeatedly observed objects (XBLs), the spectra harden systematically with increasing intensity. For seven (out of 16) XBLs, corresponding to the brightest objects in the sample, the X-ray spectrum is significantly better described by a convex, broken–power-law model than by a single power law. The results are discussed in the framework of current models for blazars.

Subject headings: BL Lacertae objects: general — quasars: general — X-rays: galaxies

1. INTRODUCTION

BL Lacertae objects are active galactic nuclei (AGNs) characterized by a high degree ($>3\%$) of linear polarization in the optical, dramatic variability at almost all frequencies, and weak or absent emission lines (e.g., Angel & Stockmann 1980; Bregman 1990). Highly polarized and optically violently variable quasars (HPQs and OVVs) share with BL Lac objects the properties associated with a strong nonthermal continuum but, at the same time, exhibit spectral features typical of ordinary quasars, such as emission lines and the blue bump. While the lack of these features represents an intrinsic difference between BL Lac objects and HPQs (e.g., Padovani 1992; Ghisellini et al. 1993), there seems to be a substantial continuity between the two classes from the point of view of the nonthermal component, hence the definition of blazars to include all the sources where the observed continuum is dominated by nonthermal emission.

The spectral energy distribution of blazars, extending smoothly from the radio to the ultraviolet band, is thought to derive from synchrotron radiation from a relativistic jet pointing close to the line of sight (Blandford & Rees 1978). In the X-ray band the situation is less clear. The synchrotron and inverse Compton processes are the most likely explanations (e.g., Jones, O'Dell, & Stein 1974; Ghisellini, Maraschi, & Treves 1985). The first mechanism requires very high magnetic fields and particle energies; the latter is bound to the radiation energy density in the source, which depends strongly on the beaming factor. The two processes may coexist, and one or the other may prevail in individual objects or statistically in a class of objects. The X-ray spectra and variability expected in the two cases are quite different. Therefore, a study of the X-ray properties of blazars is crucial for understanding the physical conditions in these sources. In addition, the recent detection of a number of blazars in γ-rays (e.g., Hunter et al. 1993; Hartman et al. 1993; Thompson et al. 1993) makes the study of the X-ray to γ-ray connection of particular interest.

BL Lac objects are well-known X-ray emitters (Schwartz et al. 1979; Schwartz & Ku 1983). A number of them have been discovered in X-ray surveys (Piccinotti et al. 1982; Stocke et al. 1991; Giommi et al. 1991). X-ray–selected BL Lac objects (XBLs) seem to differ from the radio-selected BL Lac objects (RBLs) in many properties (Stocke et al. 1985; Ledden & O'Dell 1985; Stocke et al. 1990), except that the X-ray luminosity distributions are similar (Maraschi et al. 1986; Padovani & Urry 1990).

Our knowledge of the X-ray spectra of BL Lac objects is still rather limited. From a sample of 13 objects, observed with the *Einstein* imaging proportional counter (IPC), Madejski & Schwartz (1989) found an average photon index of ~ 2.1 in the energy range 0.2–4 keV. In a review of *EXOSAT* results obtained by different authors for some (12) individual objects,

[1] Present address: Space Telescope Science Institute, 3700 San Martin Drive, Baltimore MD 21218; sambruna@stsci.edu.

Maraschi & Maccagni (1988) gave a mean value of ~ 2.5 in 0.1–10 keV. The *Ginga* distributions of three XBLs gave an average slope of ≥ 2.7 in the 2–35 keV range (Ohashi 1989), while for two RBLs a mean of ~ 1.8 was found.

Evidence for downward curvature was found by Madejski & Schwartz (1989) for a sample of six objects, using simultaneous *Einstein* IPC and MPC data. Convex spectra were also seen in the *EXOSAT* observations of PKS 0548−322 (Barr, Giommi, & Maccagni 1988). Downward curvature was indicated to be a general property of BL Lac objects by Barr et al. (1989), based on the cumulative analysis of 17 objects.

Deviations from the above behavior, e.g., the presence of a hard tail, were reported in a few cases. For the bright object PKS 2155−304 a flattening of the spectrum above 10 keV was detected in the *HEAO 1* data (Urry & Mushotzky 1982) but not confirmed by observations at later epochs (Ohashi et al. 1989; Treves et al. 1989; Sembay et al. 1993). A hard tail was recently detected in BL Lac itself (Kii et al. 1991).

Within the blazar class there seems to be some difference in the X-ray spectral shape of the different subgroups. An interesting comparison was performed for a sample of BL Lac objects (six XBLs and 24 RBLs), highly polarized quasars (HPQs) (12), and flat radio spectrum quasars (19) by Worrall & Wilkes (1990), on the basis of the *Einstein* IPC spectra, indicating that the BL Lac objects have, on average, steeper slopes than the latter two groups. This result refers to a relatively soft energy range (0.1–2.4 keV).

The *EXOSAT* satellite instrumentation comprising a low-energy (LE; 0.04–2.0 keV) imaging telescope and a medium-energy (ME; 1–20 keV) proportional counter, had an effective range of almost two decades and was therefore well suited to gather broad-band spectral information (White & Peacock 1988). In order to have a complete and uniform data set, we systematically analyzed all the spectra from the *EXOSAT* database referring to blazars. These include 93 observations for 26 blazars (16 XBLs, five RBLs, and five HPQs). Results of four BL Lac objects appearing in the *HEAO 1* all-sky survey were presented in a separate paper (Sambruna et al. 1993, hereafter S93). Of the 93 spectra used here, 22 are unpublished. A complete description of the analysis, together with spectral fits to *each of the 93 observations* is given in a separate paper (Sambruna et al. 1994, hereafter Paper I).

Here we use the results reported in Paper I to discuss the spectral properties of each object and of different classes of objects. In the case of four repeatedly observed XBLs, spectral variability is examined. The paper is structured as follows. In § 2 we summarize the information about the data set and the spectral fits. The average results for individual objects are reported in § 3, where also the spectral variability of the better-observed XBLs is addressed. The average properties of the different classes of blazars are compared in § 4. The principal findings are discussed in § 5.

2. ANALYSIS

2.1. *Data Set*

A full discussion of the adopted criteria and of the procedure of data reduction is given in Paper I and S93. Briefly, using a number of published blazar lists, we searched the *EXOSAT* database for observations useful for spectral analysis. All the objects having at least one ME spectrum of sufficient quality to allow for spectral fitting were retained. In all cases a source was also significantly ($\geq 3\ \sigma$) detected in the LE experiment. Few cases of possible confusion (more than one source in the LE field) occurred; these are discussed in Paper I. The resulting list of objects is reported in Table 1A, with the number of observations used (in parentheses), the redshifts (col. [2]), and some references for the previously published *EXOSAT* data (col. [13]). The classification of BL Lac objects as RBL or XBL is based on the ratio between the X-ray and the radio fluxes (Ledden & O'Dell 1985). The distinction between HPQs and BL Lac objects is sometimes ambiguous. We included PKS 0537−441 in the HPQ group, since a broad Mg II line of high luminosity has been observed, while PKS 0521−365 was included in the RBL group, since the observed lines are narrow and of low luminosity (Paper I).

It is clear from the above that the objects considered do not represent a statistically complete sample in the sense of a flux-limited survey. Nevertheless, from the point of view of the X-ray spectral properties they are a representative sample, since they include all the blazars observed with *EXOSAT*.

2.2. *Spectral Fits*

In Paper I we considered both the ME spectra alone and the combined LE + ME data, obtained by adding the LE data points from the various filters to the ME spectra. Each spectrum was fitted with a single power law with absorption, either fixed at the Galactic value (model a1) or allowed to vary (model a2). In most cases, the resulting χ^2 was unacceptably high. In addition, the column densities obtained with the latter model were found to be slightly higher than the Galactic values, and the spectral slopes from fitting the ME + LE data flatter than those obtained from the ME data alone. This motivated us to consider spectral models allowing for a possible convex spectrum. We therefore considered a broken–power-law model (model b) and a single–power-law model with a low-energy absorption edge (model c). In fact, in a large number of cases (40%), corresponding to the best exposed spectra, model b gives significantly better fits than model a1 and in most cases better than model c. For completeness we give here the analytical expressions adopted for model b:

$$\frac{dN}{dE} = N \times \begin{cases} \exp\left[-N_{\rm H}\,\sigma(E)\right] \times E^{-\Gamma_1} & \text{if } E < E_0\,, \\ \exp\left[-N_{\rm H}\,\sigma(E)\right] \times E_0^{\Gamma_2-\Gamma_1} E^{-\Gamma_2} & \text{if } E > E_0\,, \end{cases}$$

where Γ_1 and Γ_2 are the photon indices below and above the break energy E_0, respectively.

The results of the fits to all individual observations with the above models are reported in Paper I. In the following we report the results obtained combining individual observations of each object and groups of objects using the cumulative χ^2 statistics as described by Barr et al. (1989). The statistical significance of a χ^2 improvement was estimated using the F-test (Bevington 1969), with the standard threshold at $P_F = 95\%$. The acceptance probability P_{χ^2} test was also adopted.

3. RESULTS

In order to obtain fluxes and spectral parameters appropriate for individual objects we have to average over different observations. A first approach is to take the weighted average of the values and the corresponding weighted error, derived from individual errors estimated on the basis of confidence contours. The resulting weighted errors are usually quite small.

However, in at least four cases (Mrk 421, Mrk 501, PKS 2005−489, and PKS 2155−304, that is, the brightest and best observed objects), there is clear evidence of variability not only

in the fluxes but also in the spectral parameters. This means that values derived from different observations differ more than expected from the errors on individual observations. In these cases the only meaningful way of characterizing the spectral shape of each object is to take a simple mean and assign the corresponding rms dispersion as uncertainty. In fact, in order to estimate a 90% confidence uncertainty we multiplied the rms dispersion by 1.6.

In other cases variability may be suspected, though not definitely proved. We therefore computed both weighted averages and simple means, and associated errors for the relevant quantities. The results are reported in Table 1. Columns (1) and (2) give the name of the object (the number of used observations is reported in parentheses) and its redshift. For each object with more than one observation the first line reports the weighted averages and 90% errors, the second line the simple means and 1.6 rms dispersions for the relevant quantities. The average flux densities at 1 keV, obtained from the fits to the LE + ME data with modal a1, are given in column (3). The comparison of the measurement error and dispersion gives clear evidence for large variability for the four well-observed XBLs. A study of the temporal variability was performed by Giommi et al. (1990). For the objects with only one spectrum, we report in Table 1 the fitted parameters with the measurement errors.

The spectral index obtained from fitting the 0.1–10 keV data (LE + ME) for each object with a single power law (model a1), averaged as described above, is given in column (4). Columns (5)–(6) give the reduced χ_r^2 per degree of freedom and the corresponding acceptance probabilities for model a1, obtained combining all the available observations The χ^2 values and degrees of freedom were obtained by adding the corresponding single χ^2 values and degrees of freedom.

Spectral indices, averaged as above, break energies, χ_r^2/dof, and acceptance probabilities for the broken-power-law model (model b), are given in columns (7)–(11). Because the break energy is poorly determined in some individual observations (see Paper I, a simple average of this parameter is given in Table 1 (col. [9]). The errors are the 1.6 rms dispersions. Column (12) gives the probability P_F that the χ^2 improvement of model b with respect to model a1 is significant. We report only the cases in which P_F is greater than or equal to the standard threshold of 95%.

For Mrk 421, Mrk 501, PKS 2005−489, and PKS 2155−304, for which there is significant evidence of spectral variability, we report in Table 1B the average parameters for different intensity states, defined by grouping the observations in steps of 0.3 in the logarithm of the 2–6 keV flux (see § 3.2 for more details).

In order not to underestimate the error on the average spectral index, in the following we will use, for the spectral parameters of all objects with more than one observation, the simple mean and the corresponding 1.6 rms dispersion uncertainty.

3.1. *XBLs*

The distribution of the photon indices derived with the single–power-law model a1 for XBLs is shown in Figure 1 (*solid line*). For comparison, the photon indices derived from the fits with model a2 (free N_H) to the same data (*dashed line*) and with model a1 to the ME data only (*dotted line*) are also plotted in a separate panel. In all cases the derived photon indices are rather steep, ranging mostly between 2.0 and 3.0. The average photon indices for the ME data with model a1 and for the LE + ME data with models a1 and a2 are 2.49, 2.30, and 2.42, respectively, while the corresponding standard deviations are 0.41, 0.32, and 0.34.

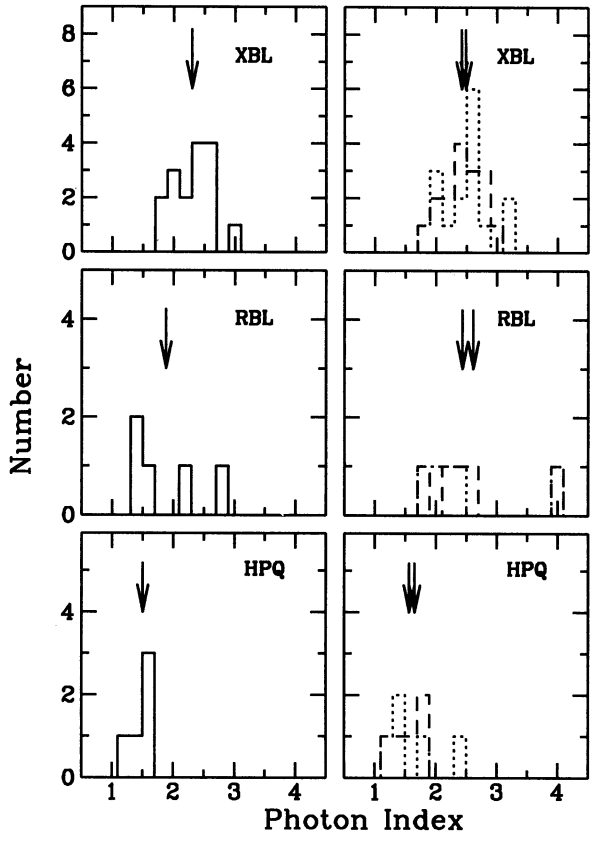

FIG. 1.—Distributions of spectral indices from the fits with single–power-law models for the different classes of sources. *Solid line:* fit to the LE + ME data with fixed N_H. *Dashed line:* fit to the LE + ME data with free N_H. *Dotted line:* fit to the ME data with fixed N_H. The arrows mark the positions of the mean values. The distributions have been obtained from the simple mean values reported in Table 1A. Irrespective of the fitted model, the XBL distributions span a range of steeper values than for HPQs.

For seven out of 16 XBLs, the average spectrum is better described by the broken–power-law model with high significance ($P_F \gtrsim 99.9\%$); these include the brighter sources in the XBL group. Downward curvature is found in all cases, that is, the spectrum steepens at high energies. Among the remaining nine objects, for I Zw 186 neither the single power law nor the broken power law is acceptable (see below). For MS 0317+18 only the broken power law is acceptable. For the other seven sources both the single–power-law and the broken–power-law models are acceptable, with a marginal improvement of the χ^2 for the second model (except for EXO 0507−04 and MS 1402+04). If the F-test is performed for the cumulated χ^2 of this group of objects, the broken power law gives a highly significant improvement.

The results of cumulating *all* the XBL spectra are reported in Table 2. We also report the results obtained for model a2 and model c (see below). Separate values are given for Mrk 421 and PKS 2155−304, for which the statistics are higher. From Table 2 it is apparent that the single–power-law models a1 and a2 are inadequate, while the broken–power-law model is acceptable as a general model for the class.

Because of the lack of spectral resolution in the LE experiment, the curvature observed in the spectra of XBL could be due to some low-energy discrete absorption. For this reason

TABLE 1A

BLAZARS OBSERVED BY *EXOSAT*
A. AVERAGE SPECTRAL PARAMETERS

Object (1)	z (2)	$\langle F_{1\,keV}\rangle$ (3)	$\langle\Gamma\rangle$ (4)	χ_r^2/dof (5)	P_{χ^2} (%) (6)	$\langle\Gamma_1\rangle$ (7)	$\langle\Gamma_2\rangle$ (8)	$\langle E_0\rangle$ (9)	χ_r^2/dof (10)	P_{χ^2} (%) (11)	P_F (%) (12)	References (13)
XBLs												
MS 0317+18 (2)	0.190	1.77 ± 0.26	1.80 ± 0.15	1.46/40	3.02	1.70 ± 0.18	~ 4.28		1.31/38	9.56	...	1
		2.28 ± 1.76	1.805 ± 0.011			1.67 ± 0.11	4.28 ± 4.22	4.0 ± 2.3				
H0323+022 (2)	0.147	3.96 ± 0.23	2.53 ± 0.07	0.72/33	88.11	2.42 ± 0.11	2.91 ± 0.50		0.70/31	89.22	...	2
		3.96 ± 0.09	2.55 ± 0.40			2.52 ± 0.42	3.93 ± 3.26	3.0 ± 2.3				
H0414+009 (4)	0.287	5.78 ± 0.23	2.08 ± 0.04	0.99/107	51.10	2.08 ± 0.10	1.97 ± 0.08		0.88/103	80.27	...	2
		5.81 ± 0.74	2.08 ± 0.32			2.08 ± 0.22	2.24 ± 0.69	2.0 ± 1.3				
EXO 0507−04 (1)	0.304	$2.99^{+0.80}_{-0.85}$	1.77 ± 0.26	0.60/13	85.64	$1.82^{+0.31}_{-0.42}$	$-1.25^{+11.25}_{-4.75}$	5.0	0.62/12	82.72	...	
PKS 0548−322 (3)	0.069	5.88 ± 0.08	2.00 ± 0.02	2.10/79	6.0×10^{-6}	1.97 ± 0.03	2.31 ± 0.10		0.97/73	55.1	>99.9	3
		7.14 ± 2.13	1.99 ± 0.03			1.89 ± 0.16	2.72 ± 1.10	3.3 ± 2.7				
Mrk 421 (14)	0.031	13.81 ± 0.10	2.38 ± 0.01	1.56/346	$<10^{-9}$	2.30 ± 0.01	2.37 ± 0.03		1.06/321	22.02	>99.9	4
		18.07 ± 22.24	2.55 ± 0.38			2.56 ± 0.42	2.71 ± 1.55	2.7 ± 2.5				
Mrk 180 (3)	0.046	2.51 ± 0.16	2.41 ± 0.05	1.16/50	20.41	2.35 ± 0.09	2.62 ± 0.72		1.04/47	39.74	...	5
		2.76 ± 304	2.55 ± 0.38			2.39 ± 0.18	3.55 ± 2.13	2.3 ± 0.9				
2A 1218+304 (3)	0.130	8.54 ± 0.14	2.14 ± 0.02	2.47/76	$<10^{-9}$	2.04 ± 0.04	2.46 ± 0.08		1.32/70	4.0	>99.9	5
		8.95 ± 1.98	2.14 ± 0.09			2.03 ± 0.16	2.49 ± 0.22	2.1 ± 0.3				
MS 1402+04 (2)	0.210	0.90 ± 0.10	2.24 ± 0.09	1.00/23	46.08	2.03 ± 0.70	2.50 ± 0.62		1.06/21	38.47	...	1
		0.96 ± 0.53	2.21 ± 0.26			1.62 ± 0.35	2.80 ± 0.32	1.0				
E1415+22 (1)	0.237	4.28 ± 0.20	2.37 ± 0.05	0.86/12	58.80	$1.72^{+0.55}_{-0.63}$	$2.77^{+0.47}_{-0.45}$	1.0	0.61/11	82.20	...	1
H1426+428 (2)	0.129	12.92 ± 0.27	2.03 ± 0.02	1.06/54	35.58	1.99 ± 0.02	2.88 ± 0.55		0.77/50	88.20	>99.9	6, 2
		12.69 ± 1.65	2.00 ± 0.13			1.97 ± 0.09	4.18 ± 1.73	5.4 ± 0.6				
Mrk 501 (10)	0.034	13.75 ± 0.09	2.28 ± 0.01	1.73/265	$<10^{-9}$	2.15 ± 0.01	2.41 ± 0.03		0.93/247	77.8	>99.9	5, 7
		12.98 ± 3.82	2.34 ± 0.22			2.30 ± 0.29	2.62 ± 0.59	2.2 ± 1.2				
H1722+119 (1)	...	3.60 ± 0.32	2.35 ± 0.09	1.10/21	33.87	2.20 ± 0.24	$2.63^{+0.38}_{-0.36}$	2.0	1.00/20	45.80	...	2
I Zw 186 (2)	0.055	3.93 ± 0.16	2.39 ± 0.05	1.93/36	0.07	2.35 ± 0.10	2.38 ± 0.23		1.57/34	1.84	...	8
		3.40 ± 0.72	2.36 ± 0.13			2.51 ± 0.45	2.30 ± 1.07	1.5 ± 0.8				
PKS 2005−489 (5)	0.071	6.31 ± 0.20	2.73 ± 0.02	1.38/105	0.60	2.69 ± 0.03	3.08 ± 0.09	3.0 ± 0.6	0.92/98	70.11	>99.9	9
		14.64 ± 25.94	2.97 ± 0.42			2.95 ± 0.67*	3.55 ± 1.66*	2.5 ± 1.8				
PKS 2155−304	0.116	28.50 ± 0.10	2.57 ± 0.01	3.67/362	$<10^{-9}$	2.59 ± 0.01	2.65 ± 0.03		1.26/340	0.09	>99.9	10
		44.14 ± 34.35	2.57 ± 0.19			2.57 ± 0.21	2.78 ± 0.43	2.8 ± 2.2				
RBLs												
3C 66A (3)	0.444	0.62 ± 0.08	1.43 ± 0.08	1.97/43	0.02	0.92 ± 0.24	2.53 ± 0.35		0.93/40	59.70	>99.9	11
		0.64 ± 0.32	1.45 ± 0.34			0.80 ± 0.91	4.10 ± 4.46	1.6 ± 0.8				
PKS 0521−365 (2)	0.055	1.58 ± 0.14	1.58 ± 0.07	0.86/45	73.46	1.51 ± 0.11	2.63 ± 0.72		0.67/42	95.00	97.5	8
		1.63 ± 0.35	1.60 ± 0.18			1.49 ± 0.19	2.77 ± 0.80	3.8 ± 0.5				
PKS 0754+100 (1)	...	$0.72^{+0.17}_{-0.11}$	1.31 ± 0.14	1.6/13	7.70	0.99 ± 0.47	2.00 ± 0.96	2.0	1.48/12	12.32	...	
OJ 287 (2)	0.306	2.16 ± 0.15	2.27 ± 0.07	2.79/29	$<10^{-9}$	2.01 ± 0.20	2.88 ± 0.78		2.17/25	0.06	...	
		2.16 ± 0.17	2.36 ± 0.24			1.96 ± 0.80	3.51 ± 2.03	2.0				
3C 371 (2)	0.050	1.97 ± 0.15	2.79 ± 0.07	1.31/41	8.82	3.85 ± 0.44	1.86 ± 0.41		0.72/38	89.96	>99.9	12
		1.98 ± 1.33	2.80 ± 0.14			3.81 ± 0.21	1.86 ± 0.00	0.9 ± 0.1				
HPQs												
PKS 0537−441 (1)	0.894	$0.40^{+0.40}_{-1.51}$	1.26 ± 0.28	0.4/20	99.18	$1.46^{+1.44}_{-3.28}$	$1.44^{+0.68}_{-0.71}$	1.0	0.56/19	93.53	...	13
Ton 599 (3)	0.729	0.62 ± 0.06	1.64 ± 0.14	0.83/50	79.84	1.43 ± 0.34	2.11 ± 0.51		0.87/47	72.25	...	
		0.69 ± 0.35	1.66 ± 0.06			1.30 ± 0.89	2.11 ± 0.26	1.3 ± 0.9				
PKS 1510−08 (3)	0.361	0.84 ± 0.07	1.46 ± 0.08	1.21/72	10.82	1.33 ± 0.15	1.89 ± 0.32		1.19/70	13.23	...	14
		0.84 ± 0.05	1.46 ± 0.21			1.08 ± 0.78	1.96 ± 1.37	3.5 ± 5.6				
3C 390.3 (5)	0.056	1.67 ± 0.08	1.49 ± 0.03	1.53/125	0.01	1.35 ± 0.12	1.68 ± 0.09		0.89/119	79.9	>99.9	15
		2.71 ± 1.98	1.48 ± 0.22			1.18 ± 0.56	2.00 ± 0.77	2.5 ± 1.4				
PKS 2208−137 (1)	0.392	$0.96^{+0.25}_{-0.26}$	1.66 ± 0.26	0.9/21	59.16	$1.68^{+0.46}_{-0.52}$	$1.54^{+2.14}_{-1.54}$	3.0	0.98/20	48.32	...	

TABLE 1—*Continued*

B. REPEATEDLY OBSERVED XBLs[a]

Object (1)		z (2)	$\langle F_{1\ keV}\rangle$ (3)	$\langle\Gamma\rangle$ (4)	χ_r^2/dof (5)	P_{χ^2} (%) (6)	$\langle\Gamma_1\rangle$ (7)	$\langle\Gamma_2\rangle$ (8)	$\langle E_0\rangle$ (9)	χ_r^2/dof (10)	P_{χ^2} (%) (11)	P_F (%) (12)
Mrk 421	A (2)	0.031	7.88 ± 0.63	2.83 ± 0.06	1.24/32	16.5	2.92 ± 0.13	2.04 ± 0.48		1.11/28	31.4	...
			6.91 ± 2.26	2.84 ± 0.03			2.87 ± 0.22	2.73 ± 1.74	2.15 ± 0.05			
	B (6)		10.31 ± 0.13	2.64 ± 0.09	1.10/138	19.93	2.68 ± 0.02	2.50 ± 0.10		0.99/128	51.5	95
			11.48 ± 4.96	2.67 ± 0.14			2.66 ± 0.13	3.01 ± 2.26	3.2 ± 2.9			
	C (3)		13.95 ± 0.18	2.50 ± 0.05	1.45/80	0.53	2.53 ± 0.03	2.40 ± 0.05		1.00/75	47.8	>99.9
			14.02 ± 1.79	2.50 ± 0.08			2.60 ± 0.13	2.42 ± 0.26	1.1 ± 1.3			
	D (3)		42.54 ± 0.35	2.15 ± 0.02	2.42/96	$<10^{-9}$	2.12 ± 0.01	2.32 ± 0.04		1.20/90	9.51	>99.9
			42.78 ± 9.33	2.16 ± 0.03			2.12 ± 0.03	2.40 ± 0.22	3.6 ± 1.1			
Mrk 501	A (1)	0.034	9.37 ± 0.46	2.62 ± 0.04	0.8/27	75.74	2.69 ± 0.07	2.34 ± 0.24	$2.3^{+6.8}_{-1.5}$	0.73/25	83.1	...
	B (4)		11.26 ± 0.17	2.40 ± 0.05	1.21/110	6.62	2.38 ± 0.03	2.56 ± 0.10		1.00/102	48.1	>99.9
			11.38 ± 0.56	2.40 ± 0.08			2.36 ± 0.06	2.84 ± 0.74	2.6 ± 1.4			
	C (5)		15.06 ± 0.11	2.25 ± 0.06	2.37/128	$<10^{-9}$	2.07 ± 0.01	2.40 ± 0.03		0.93/117	99.9	>99.9
			15.00 ± 2.22	2.23 ± 0.09			2.17 ± 0.09	2.51 ± 0.43	1.9 ± 1.1			
PKS 2005−489	A (3)	0.071	3.07 ± 0.22	3.16 ± 0.20	0.51/49	99.83	3.12 ± 0.14	2.99 ± 0.44		0.43/46	99.97	...
			3.52 ± 2.74	3.12 ± 0.32			3.18 ± 0.82*	4.04 ± 2.42*	2.7 ± 2.5			
	B (2)		27.95 ± 0.56	2.70 ± 0.18	2.15/56	$<10^{-9}$	2.66 ± 0.03	3.09 ± 0.09	3.0 ± 0.6	1.36/52	4.31	>99.9
			31.32 ± 17.36	2.75 ± 0.29			2.69 ± 0.29	3.06 ± 0.03	3.0 ± 1.6			
PKS 2155−304	A (2)	0.116	17.54 ± 0.14	2.71 ± 0.04	2.87/38	$<10^{-9}$	2.71 ± 0.01	3.14 ± 0.17		1.94/35	0.07	97.5
			17.54 ± 10.37	2.71 ± 0.06			2.70 ± 0.05	2.84 ± 0.70	4.1 ± 1.8			
	B (5)		33.80 ± 0.17	2.65 ± 0.05	2.19/123	$<10^{-9}$	2.61 ± 0.01	2.79 ± 0.11		1.13/116	16.02	>99.9
			33.00 ± 6.51	2.66 ± 0.08			2.65 ± 0.13	2.93 ± 0.43	2.7 ± 2.1			
	C (6)		48.52 ± 0.32	2.55 ± 0.08	1.49/144	0.01	2.56 ± 0.02	2.55 ± 0.05		1.09/136	22.3	>99.9
			47.66 ± 13.79	2.52 ± 0.13			2.52 ± 0.14	2.66 ± 0.46	2.1 ± 2.2			
	D (2)		86.62 ± 0.59	2.40 ± 0.11	12.86/57	$<10^{-9}$	2.41 ± 0.01	2.83 ± 0.06		1.53/53	0.78	>99.9
			88.02 ± 5.26	2.41 ± 0.18			2.37 ± 0.16	2.86 ± 0.06	3.6 ± 1.7			

NOTE.—An asterisk means value does not include the 85/145 observation (see Paper I).

EXPLANATION OF COLUMNS.—(1) Source name. Number of observations used in parenthesis. (2) Redshift. (3) Average flux at 1 keV (in μJy). First line: weighted average and 90% error. Second line: simple mean and 1.6 rms. (4) Photon index from fits with power law plus Galactic absorption. Lines as in col. (3). (5) Cumulative χ^2 for the power law + Galactic absorption model. (6) Probability for a random data set exceeding χ^2. (7) From broken–power-law fits: low-energy photon index. Lines as in col. (3). (8) From broken–power-law fits: high-energy photon index. Lines as in col. (3) (9) Break energy, in keV. Lines as in col. (3). The weighted averages are calculated from the errors at 67%, when available (Paper I). (10) Cumulative χ^2 for the broken–power-law model. (11) Probability for a random data set exceeding χ^2. (12) Significance of the χ^2 improvement (from the F-test). (13) Selected references for the previously published spectra.

[a] The intensity states for the four objects listed in Table 1B were obtained grouping the following spectra (Paper I): Mrk 421: A = 84/033, 84/035; B = 84/032, 84/037, 85/004, 85/126, 85/132, 85/141, C = 85/112, 85/118, 85/131; D = 84/337, 84/338, 84/340. Mrk 501: A = 84/207; B = 84/183, 84/191, 84/201, 85/099; C = 84/034, 84/036, 84/086, 84/209, 86/074. PKS 2005−489: A = 85/145, 85/276, 85/289; B = 84/254, 84/287. PKS 2155−304: A = 83/304, 85/316; B = 83/333, 84/311A, 84/312A, 85/305, 85/306; C = 84/311B, 84/311C, 84/311D, 84/312B, 84/312C, 84/316; D = 84/312D, 85/297.

REFERENCES.—(1) Giommi et al. 1987; (2) S93; (3) Barr, Giommi, & Maccagni 1988; (4) George, Warwick, & Bromage 1988a; (5) George, Warwick, & McHardy 1988b; (6) Remillard et al. 1989; (7) Staubert et al. 1986; (8) Garilli & Maccagni 1990; (9) Wall et al. 1986; (10) Treves et al. 1989; (11) Maccagni et al. 1987; (12) Staubert, Brunner, & Worrall 1986; (13) Treves et al. 1993; (14) Singh, Rao, & Vahia 1990; (15) Ghosh & Soundararajaperumal 1991.

TABLE 2

CUMULATIVE RESULTS

OBJECTS	MODEL a1 POWER LAW, FIXED N_H		MODEL a2 POWER LAW, FREE N_H		MODEL b BROKEN POWER LAW			MODEL c POWER LAW + EDGE		
	χ_r^2/dof	P_{χ^2}	χ_r^2/dof	P_{χ^2}	χ_r^2/dof	P_{χ^2}	P_F[a]	χ_r^2/dof	P_{χ^2}	P_F[a]
XBLs (all)[b]	1.53/914	$<10^{-9}$	1.12/873	9×10^{-3}	0.98/855	0.61	>0.999	1.38/860	$<10^{-9}$	0.975
RBLs (all)	1.63/171	3.5×10^{-7}	1.17/161	0.07	1.05/157	0.30	>0.999	1.28/157	0.01	>0.999
HPQs (all)	1.20/288	0.01	0.98/276	0.59	0.95/275	0.70	>0.999	...	...	...
Mrk 421	1.56/346	$<10^{-9}$	1.36/332	1×10^{-5}	1.06/321	0.22	>0.999	1.16/327	2.4×10^{-2}	>0.999
PKS 2155−304	3.67/362	$<10^{-9}$	1.71/347	$<10^{-9}$	1.26/340	8×10^{-4}	>0.999	1.62/338	$<10^{-9}$	>0.999

[a] With respect to model a1.

[b] Without Mrk 421 and PKS 2155−304.

we also tried fitting with a single–power-law + low-energy absorption edge (model c), which could mimic a spectral flattening in the soft X-ray range. The results are reported in Paper I. Only in a few cases does the latter model give results superior to the broken–power-law model. This occurs for H1426+428, I Zw 186, and PKS 2005−489. In three other cases it is equivalent to the broken power law (H0414+009, EXO 0507−04, MS 1402+04). However, considering *all* the XBL spectra together, model c is not an acceptable representation of the data, although it gives a significant improvement with respect to the single–power-law model (Table 2).

We conclude that the XBL spectra in the 0.1–10 keV range are generally curved and can be described by broken power laws, while a single–power-law + low-energy feature may apply in some cases but not for the whole group.

3.2. *Repeatedly Observed XBLs*

The four bright XBLs Mrk 421, Mrk 501, PKS 2005−489, and PKS 2155−304 were observed by *EXOSAT* on several occasions with different fluxes. We grouped the observations in intensity states (cases labeled A–D) by dividing the 2–6 keV flux range for each source into logarithmic intervals of width 0.3 (see notes to Table 1). For PKS 2005−489, state A was obtained from the three low states of 85/145, 85/276, and 85/289, while state B refers to the high states of 84/254 and 84/287. The spectral parameters for each intensity state obtained with the cumulative χ^2 method are reported in Table 1B.

Comparing the slopes obtained with the single–power-law model, it is clear that for each source the spectra change systematically with intensity, becoming harder when the intensity increases. In Figures 2*a*–2*d* (*lower panels*) we plot the photon indices for each observation (from Paper I) against the 2–6 keV count rates for each object. For all sources the correlation between Γ and intensity is significant at the 99.9% level (from a Spearman-Kendall test). Note that in the case of Mrk 421 the photon index "saturates" at $\Gamma \simeq 2$ for high intensity, as found by George, Warwick, & Bromage (1988a). The behavior of PKS 2155−304 appears less regular.

The fits with the broken–power-law model yield significantly convex spectra in the highest intensity states, for all the objects, while in some of the fainter states there is no evidence of curvature. This may simply be due to insufficient statistics in the faint states, at least for Mrk 501 and PKS 2005−489.

For Mrk 421 the fit with the broken–power-law model is significantly better than the fit with the single–power-law model in the three higher states, B, C, and D, but in states B and C a concave spectrum is derived comparing the (weighted average) values of Γ_1 and Γ_2, with an indication of flattening above a few keV. This argues for a qualitative change in spectral shape.

We note that for the low states of PKS 2155−304 the power law + edge model is better than (A; $\chi_r^2 = 1.43/34$) or equivalent (B; $\chi_r^2 = 1.20/115$) to model b, while for the higher intensity states it is definitely worse (C; $\chi_r^2 = 1.28/135$; D: $\chi_r^2 = 3.50/53$).

The low-energy photon index Γ_1 for each observation is plotted in Figures 2*a*–2*d* (*upper panels*) against the 2–6 keV intensity for the cases where the determination is significant. It follows closely the behavior of the single–power-law index mentioned above. Thus the hardening cannot be attributed simply to a change in the break energy.

The fits to the single spectra with both models b and c are reported in detail in Paper I, where comparison with the previously published *EXOSAT* and with data from other satellites is also given.

3.3. *RBLs*

The distributions of spectral indices from the single–power-law fits (models a1 and a2) for RBLs are shown in Figure 1 (see figure legend). The average photon indices are 2.43, 1.88, and 2.61 for the ME data (model a1) and the LE + ME data (models a1 and a2), respectively, with corresponding standard deviations 0.90, 0.63, and 0.90. The spread is rather wide despite the small number of objects. Note the very soft spectrum of OJ 287.

The broken–power-law model is favored for three sources (3C 66A, PKS 0521−365, and 3C 371), and in the first two yields a convex spectrum. However, in 3C 66A the flattening at lower energy is probably due to absorption by intervening matter (see Paper I). In fact the fit with a single power law + free absorption is equivalent to the fit with the broken power law, and yields N_H in excess of the Galactic value. For 3C 371 the spectrum appears to be concave, showing a steep soft excess and a flatter high-energy photon index. An equivalent fit is obtained with the power-law + edge model.

Because of the limited statistics, it is difficult to make general statements on the spectral shapes of RBLs. On the other hand, from a cumulative analysis of all the RBL spectra, the broken–power-law model is significantly preferred with respect to the single–power-law model and is an acceptable representation of the data (Table 2). The power-law + edge model also yields a highly significant improvement, although the fit is still poor.

3.4. *HPQs*

The distribution of photon indices of HPQs from the fits with model a1 is shown in Figure 1 (*solid line*), together with

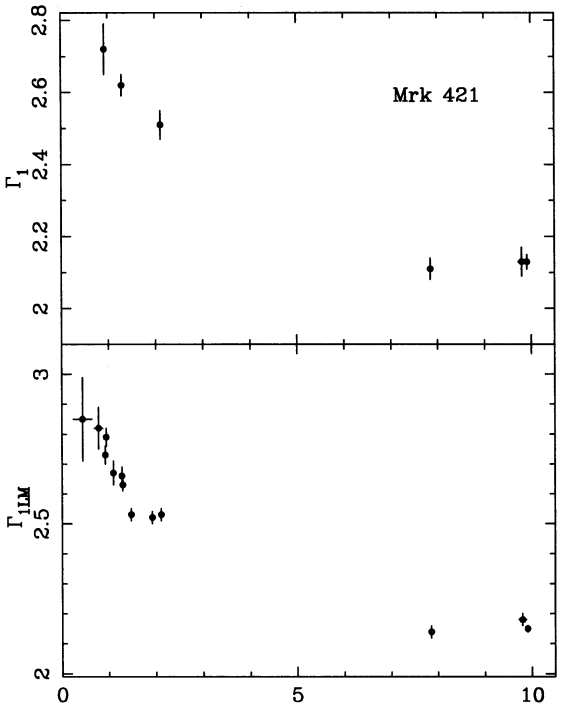

FIG. 2*a*

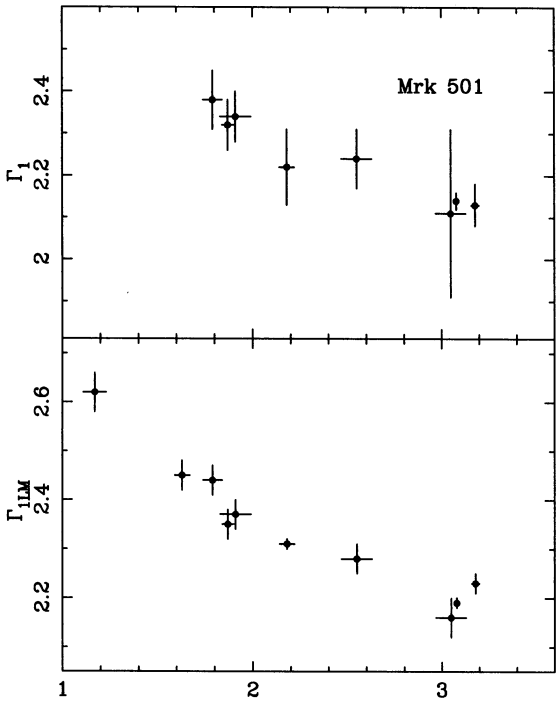

FIG. 2*b*

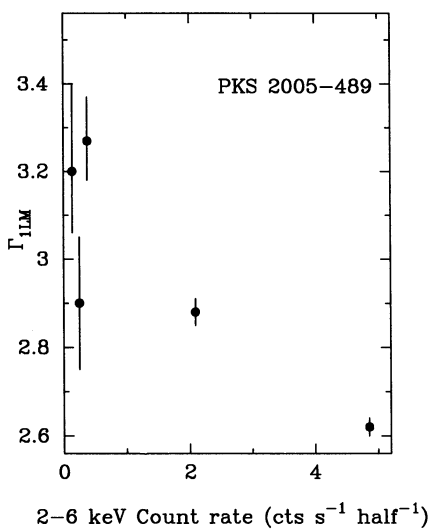

FIG. 2*c*

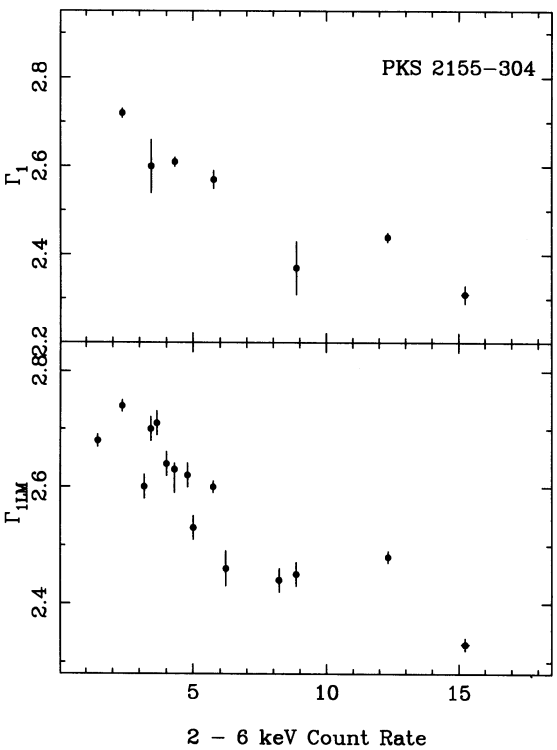

FIG. 2*d*

FIG. 2.—(*a*) Spectral variability for Mrk 421. *Lower panel:* spectral index Γ_{1LM} from the fit to the LE + ME data with a single–power-law model (N_H fixed). *Upper panel:* low-energy spectral index Γ_1 from the fit with the broken–power-law model. The values of the spectral indices refer to individual observations and are taken from Paper I. (*b*) Spectral variability for Mrk 501 (panels as in [*a*]). (*c*) Spectral variability for PKS 2005−489. The spectral index is from the fit to the individual LE + ME spectra with power-law model with fixed N_H (from Paper I). (*d*) Spectral variability for PKS 2155−304 (panels as in [a]).

the distributions obtained from the fits with the other single–power-law models (see figure legend). They fall in a remarkably narrow range (1.2–1.7), with mean 1.50 and standard deviation 0.17. The average photon indices for the ME data, model a1, and for the LE + ME data, model a2, are 1.65 and 1.56, with standard deviations 0.41 and 0.31, respectively.

From Table 1 it is apparent that the single–power-law + Galactic absorption model is a good representation of the spectra of three of the present HPQs, except for 3C 390.3 and PKS 1510−08, for which it yields a rather high χ^2. For 3C 390.3 the broken power law gives a better fit in two observations (see, however, Paper I). In the case of PKS 1510−08, possible evidence for a feature at ~ 5.0 keV is present, and the fit with the power law + a Gaussian model gives a marginal improvement (see Paper I). Comparing the results of a cumulative fitting of the whole group with models a1, a2, and b (Table 2), it is seen that for HPQs allowing N_H to vary gives an acceptable result, equivalent to introducing the broken–power-law model. We conclude that for this group there is no evidence of intrinsic curvature of the continuum, and that a single–power-law model is an adequate representation of the *EXOSAT* data.

4. AVERAGE PROPERTIES

In the following, we indicate the photon indices from the fits to the ME data with model a1 and to the LE + ME data with models a1 and a2 as Γ_{1M}, Γ_{1LM}, and Γ_{2LM}, respectively. The luminosities were calculated assuming $H_0 = 50$ km s^{-1} Mpc^{-1} and $q_0 = 0.5$. For each object we assumed the simple mean values and the rms multiplied by 1.6 (see above). Our conclusions are not affected if the weighted averages and errors are used instead.

4.1. *Spectral Index*

Comparing the spectral index distributions shown in Figure 1 for the different subgroups of blazars, it is clear that, irrespective of the fitted model, the spectral indices of XBLs are steeper than those of HPQs. The distribution for RBLs is, unfortunately, poorly defined.

A maximum-likelihood analysis (e.g., Maccacaro et al. 1988) of all the distributions, assuming that, in each case, the spectral indices have an intrinsic Gaussian distribution with center $\langle\Gamma\rangle$ and width σ, gives the results reported in Table 3A (best-fit values and 90% errors) for Γ_{1M}, Γ_{1LM}, and Γ_{2LM}. Figure 3*a*–3*c* show the 90% confidence contours in the $\langle\Gamma\rangle$-σ plane, which confirm that the X-ray spectra of HPQs are significantly flatter than those of XBLs. Again, the large uncertainties prevent any firm statement concerning RBLs. However, there is weak indication that the ME spectral indices for RBLs are flatter than for XBLs (Table 3A and Figs. 3*a*–3*b*).

In Figure 3, note that in the case of XBLs the confidence contours for Γ_{1M} and Γ_{2LM} (*dotted and dashed lines*) are nearly coincident and enclose a region of steeper spectral indices than the Γ_{1LM} contour (*solid line*). As discussed in Paper I, this indicates that the spectra are curved, and suggested to us to consider model b.

Worrall & Wilkes (1990) studied the *Einstein* IPC data for a sample of 12 HPQs, 24 RBLs and six XBLs. The average slopes reported by these authors for HPQs (1.5) and for RBLs (2.0) agree with those obtained here, while the slope obtained for XBLs (2.0) is flatter than that of Table 3A (2.2–2.4). Since the energy range of the *Einstein* IPC (0.2–3.5 keV) was lower than that of the *EXOSAT* data, this is additional evidence that the XBL spectra become steeper with increasing energy. We report in Table 3B the average spectral parameters obtained with the broken–power-law model for the seven XBLs significantly curved in Table 1. The average energy of the break, ~ 3.0 keV, is a simple mean. The low- and high-energy spectral indices were derived using the maximum-likelihood method. Although the cumulative χ^2 shows that the curvature is highly significant for the XBL class (see above), the average low- and high-energy spectral indices in Table 3B are not different within the 90% errors. This is likely to be due to the dispersion introduced by the variability of the single objects (see above).

TABLE 3

AVERAGE X-RAY PROPERTIES OF THE *EXOSAT* BLAZARS

A. SINGLE–POWER-LAW MODELS

Average Indices (1)	XBLs (2)	RBLs (3)	HPQs (4)
$\langle\Gamma_{1M}\rangle$	2.40 ± 0.20	$1.91^{+0.39}_{-0.19}$	$1.65^{+0.56}_{-0.40}$
σ	$0.19^{+0.18}_{-0.12}$	$0.0 (< 0.52)$	$0.0 (< 0.81)$
$\langle\Gamma_{1LM}\rangle$	$2.20^{+0.17}_{-0.15}$	$1.85^{+0.75}_{-0.67}$	$1.62^{+0.11}_{-0.24}$
σ	$0.21^{+0.17}_{-0.18}$	$0.52^{+0.84}_{-0.25}$	$0.0 (< 0.29)$
$\langle\Gamma_{2LM}\rangle$	$2.37^{+0.18}_{-0.17}$	$2.08^{+0.77}_{-0.53}$	$1.68^{+0.42}_{-0.58}$
σ	$0.17^{+0.18}_{-0.17}$	$0.26^{+0.89}_{-0.16}$	$0.0 (< 0.81)$

B. BROKEN–POWER-LAW MODEL

Property	XBLs[a]
$\langle E_0\rangle$ (keV)	3.03 ± 1.12
$\langle\Gamma_1\rangle$	$2.24^{+0.34}_{-0.29}$
σ_1	$0.28^{+0.35}_{-0.17}$
$\langle\Gamma_2\rangle$	$2.54^{+0.61}_{-0.34}$
σ_2	$0.0 (< 0.70)$

C. LUMINOSITY

Property (1)	XBL (2)	RBL (3)	HPQ (4)	XBL-RBL (5)	All (6)
$\langle\log L_{ME}\rangle$	44.76	44.62	45.54	44.73	44.90
σ	0.71	1.10	0.81	0.77	0.83
$\langle\log L_{LE}\rangle$	45.33	45.34	45.34	45.33	45.33
σ	0.68	1.68	0.67	0.91	0.86

[a] From the XBLs significantly curved in Table 1A.

4.2. *Luminosity*

Average X-ray luminosities were computed for all the objects of known redshift in the ME (2–6 keV) and LE (0.1–2.0 keV) ranges, assuming isotropic emission. The luminosities in the LE and ME energy ranges (L_{LE}, L_{ME}) were obtained from the incident fluxes reported in Paper I.

The histograms of the ME and LE luminosities are plotted in Figure 4 for XBLs, RBLs, and HPQs. The corresponding averages and standard deviations from a simple mean are reported in Table 3C. The histograms for XBLs, RBLs, and HPQs span similar luminosity intervals, from $10^{43.5}$ to $10^{46.5}$ ergs s^{-1}. Note the exceptionally high LE luminosity of OJ 287 (1.6×10^{47} ergs s^{-1}). The average values for the three groups of objects are indistinguishable at the present level of statistics (Table 3C). It should be noted, however, that four HPQs are among the most luminous objects in the sample, and the one at low luminosity, 3C 390.3, may be a spurious classification (e.g.,

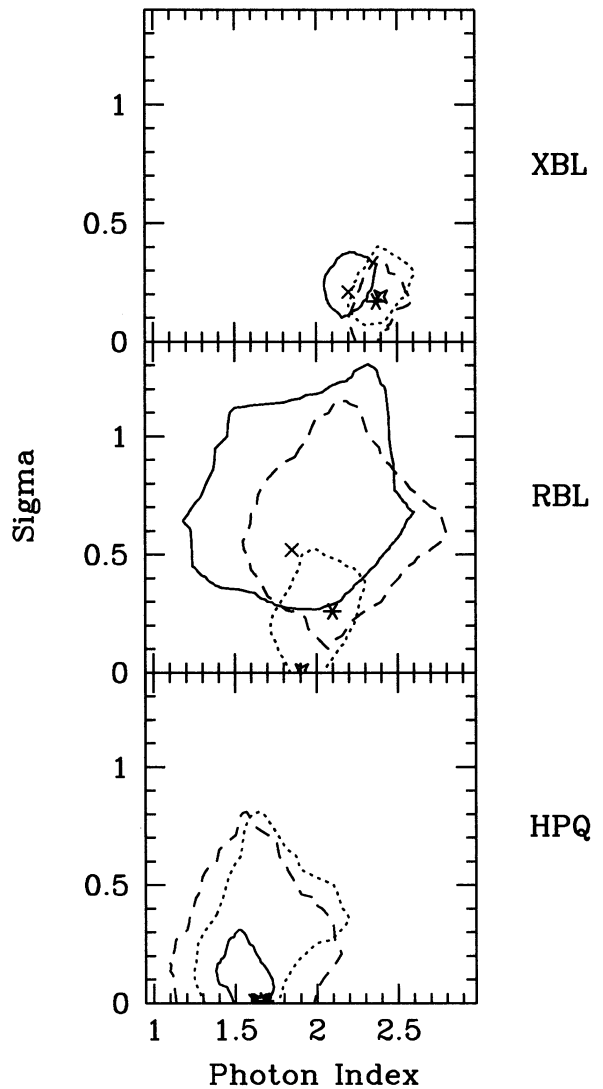

FIG. 3.—Best-fit (*symbols*) and 90% contours from the maximum-likelihood test. The spectral indices (simple means + 1.6 rms dispersions) are from the fit with single–power-law models. *Solid line and cross:* fit to the LE + ME data with fixed N_H. *Dashed line and asterisk:* fit to the LE + ME data with free N_H. *Dotted line and star:* fit to the ME data with fixed N_H. The HPQ group is characterized by flatter spectra than the XBL group.

Eracleous & Halpern 1993). If so, one could argue that HPQs are more luminous with respect to BL Lac objects.

In summary, no significant difference in X-ray luminosity distribution is apparent between XBLs and RBLs, which span the same interval in both the LE and the ME energy bands. This confirms the previous findings of Maraschi et al. (1986), based mainly on *Einstein* data gathered from the literature for a larger sample of objects.

4.3. *Correlations*

We searched for possible correlations between the spectral slopes obtained from single–power-law fits (Γ_{1M}, Γ_{1LM}) and the luminosities (L_{LE}, L_{ME}) for the three groups of blazars. Using the Spearman-Kendall rank tests, we found only the correlation between Γ_{1LM} and L_{ME} to be significant (99.67%), as is shown in Figure 5. For the dominant class of the BL Lac objects the above tests give a correlation significance of 95.32%. Two objects deviate strongly from the general trend. These are the RBL PKS 0521−365 and the HPQ 3C 390.3, whose classifications are uncertain (see above).

The displayed trend is a harder spectral index at higher luminosity. Note that this correlation is absent when the average slopes are plotted against the average fluxes. The trend is analogous to the spectral behavior found for single XBLs observed at different intensity states (see above).

5. DISCUSSION

The results presented above are of two types. On one hand, it is found that the X-ray spectra of XBLs are steep and convex, with a clear trend of flattening with increasing intensity for the best-observed objects. On the other hand, the spectra of HPQs, though limited to a few objects, are definitely flatter than those of XBLs, as previously observed by Worrall & Wilkes (1990) in the (softer) *Einstein* band. Among the five RBLs in the sample we find very different spectra, and no general statement is possible.

The average X-ray properties of BL Lac objects are distinct with respect to those of Seyfert galaxies and quasars. Seyfert galaxies and radio-loud and radio-quiet quasars studied in the *EXOSAT* ME band have average slopes ~1.7, 1.6, and 1.9, respectively (Turner & Pounds 1989; Lawson et al. 1992), while for BL Lac objects we found ~2.4 in the same band. Moreover, the spectral variability behavior is different. In fact, for Seyfert galaxies the prevailing trend is a softening of the spectrum with increasing intensity (Grandi et al. 1992).

It is generally believed that the radiation from blazars is relativistically beamed (Blandford & Rees 1978) and comes from an elongated jetlike structure pointing to the observer (Marscher 1980; Königl 1981). From the radio to the optical band the emission mechanism is supposedly synchrotron radiation, but several components are required to explain the flat radio spectra, i.e., the jet is inhomogeneous. At higher energies the models are not well established. The jet may still be inhomogeneous (e.g., Ghisellini, Maraschi, & Treves 1985; Ghisellini & Maraschi 1989), or a single component may dominate. Synchrotron emission may extend up to the X-ray band, but a new component due to inverse Compton scattering is also expected.

The steep spectra of BL Lac objects, which usually connect smoothly with an extrapolation from lower frequencies, suggest that X-rays in these objects are produced via synchrotron emission. In this case the radiation derives from the highest energy electrons. If the jet is inhomogeneous the observed "curvature" in the spectra can be accounted for in terms of the inner jet structure. This requires relativistic electrons with power-law energy distributions extending to higher energies with decreasing dimensions (Ghisellini et al. 1985).

On the other hand, the spectral steepening may be interpreted as due to a balance between radiative and expansion/diffusion losses. The observed spectral variability behavior agrees with this picture, since it is expected that freshly injected electrons would show the flatter energy distribution before suffering radiative losses. However, the estimated radiative times are rather short with respect to the crossing time of the emitting region, unless the beaming factor is higher than generally estimated (e.g., Ghisellini et al. 1993).

It is interesting to note that the inner jet region may be the site of one (or more) strong relativistic shocks responsible for continuous particle acceleration. An exact solution for the transport equation which may be appropriate for this case was

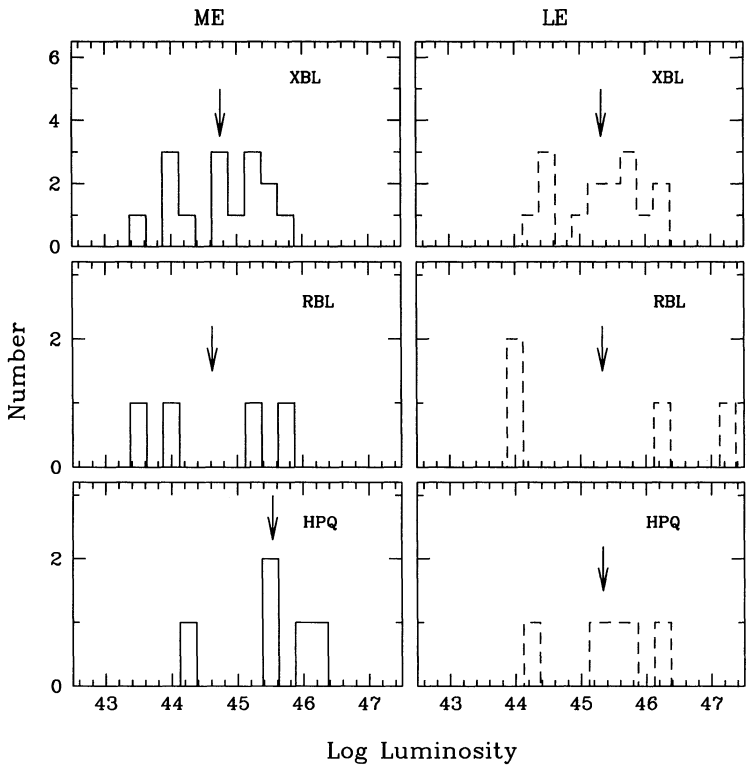

FIG. 4.—Distributions of luminosities in the ME (2–6 keV) and in the LE (0.1–2.0 keV) ranges (*solid and dashed lines, respectively*). Average values of the luminosities were considered for each source. The arrows indicate the average luminosities of the groups.

given by Bregman (1985), who showed that the integrated synchrotron spectrum is a power law at low energies, steepening gradually at high energies. The steepening expected in the model is larger than observed; however, it is conceivable that a more realistic treatment could reproduce the observed behavior. In this model the radiative losses are balanced by the shock acceleration, so that the timescale difficulty mentioned above may, perhaps, be overcome. Further work along this line is needed.

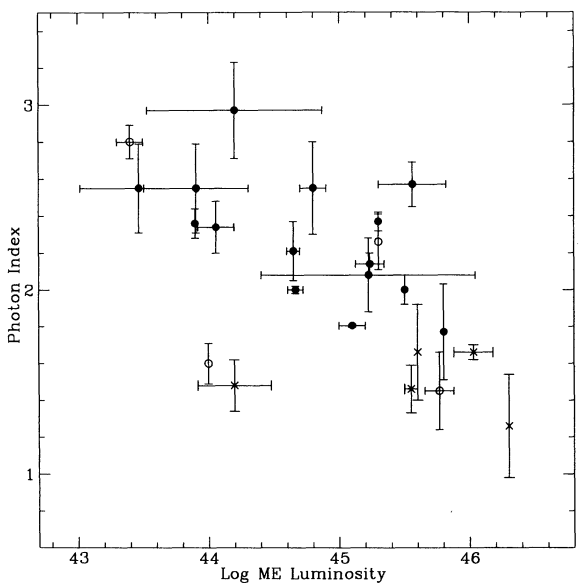

FIG. 5.—Correlation between the photon indices from the fit to the LE + ME data with a single-power-law model (fixed N_H) and the ME luminosity (2–6 keV). *Filled circles:* XBLs; *open circles:* RBLs; *crosses:* HPQs. The correlation is significant at 99.7% according to a Spearman-Kendall test, and goes in the sense of flatter spectra for higher luminosities. The RBLs and HPQs which do not follow the general trend are PKS 0521−365 and 3C 390.3, respectively.

In contrast to XBLs, HPQs have flat X-ray spectra, well above an extrapolation of the optical UV spectra, suggesting a different origin. It is natural to interpret this component as due to inverse Compton scattering of the relativistic electrons emitting the synchrotron photons either on the synchrotron photons themselves or on other photons external to the jet. A model of the latter type was examined by Melia & Königl (1989), who considered inverse Compton scattering by collimated ultrarelativistic particles on the thermal photons emitted by an accretion disk. The emergent X-ray spectrum consists of a convex component in the region below 10 keV, due to first-order Compton scattering, which mimics the shape of the thermal emission from the disk, and a flat, high-energy (>10 keV) tail, which represents the higher order scattering. Thus, an inverse Compton component in blazars is expected in several models and is a natural explanation for the flat X-ray spectra observed in HPQs.

Recently γ-rays have been detected by the EGRET experiment on board the *Compton Gamma Ray Observatory* (*GRO*) for 26 objects (Hartman 1993), four of which are part of the present sample. It is remarkable that only one, Mrk 421, belongs to the XBLs, the group which is brightest in X-rays. It is also worth recalling that Mrk 421 is the only XBL which at times shows a slight concavity (see states A, B, C in Table 1B and Paper I), which may be associated with a flat component emerging at high energy. The other three (3C 66A, PKS 0521−385, and PKS 0537−441) are among the eight objects in the sample with spectra flatter than 1.6. It is therefore likely

that the flat component observed in X-rays is directly connected with the observed γ-rays (Maraschi 1992; Treves et al. 1993).

A more subtle question is why the inverse Compton component is more prominent in HPQs than in BL Lac objects. A basic distinction between the two classes could be the presence of the UV bump and the associated broad-line region. In fact, it has been shown that most BL Lac objects have similar beaming factors and intrinsically weaker emission lines than HPQs (Padovani 1992; Ghisellini et al. 1993). If so, it would follow that the energy density of "ambient" photons as seen by the jet dominates the radiation density of synchrotron photons.

6. SUMMARY AND CONCLUSIONS

We have studied the X-ray spectra of 26 blazars in the 0.1–10 keV range, using the full *EXOSAT* database. The sample, which is not the result of a flux-limited survey, contains 16 XBLs, five RBLs, and five HPQs. Our main results are the following:

1. The X-ray spectra of XBL are steep, $\langle\Gamma\rangle = 2.20^{+0.17}_{-0.15}$. A broken–power-law model gives significantly better spectral fits for seven out of 16 objects and for the remaining ones taken cumulatively.

2. The distributions of spectral indices of XBLs and HPQs are different, HPQs having flatter slopes, $\langle\Gamma\rangle = 1.62^{+0.11}_{-0.24}$.

3. In the four XBLs for which repeated observations are available, the spectra flatten with increasing intensity. The same trend is exhibited by the low-energy photon index of the broken–power-law model.

4. For the three groups, the average spectral index is correlated with the ME luminosity, being flatter at higher luminosities.

5. The X-ray luminosity distributions span similar ranges for the three groups, although HPQs tend to cluster at the higher luminosity end.

Both the steepness of the X-ray spectra and the variability properties of XBLs are probably a consequence of the dominance of the emission from a relativistic jet, and the likely emission mechanism is synchrotron emission by continuously reaccelerated particles. The flat spectra of HPQs can be understood as highly beamed inverse Compton photons produced by scattering of the relativistic photons in the jet either on the synchrotron photons or on the thermal photons of the UV bump. Future observations with greater sensitivity in a comparable energy range, possibly simultaneous with γ-ray observations, are needed to measure the relative importance of the two components for a much wider sample.

R. M. S. is grateful to SISSA for financial support, and to ESTEC for providing the software used for the analysis. J. E. Pesce is thanked for a careful reading of the manuscript. We acknowledge an anonymous referee for valuable comments.

REFERENCES

Angel, R., & Stockmann, H. S. 1980, ARA&A, 18, 321
Barr, P., Giommi, P., & Maccagni, D. 1988, ApJ, 324, L11
Barr, P., Giommi, P., Pollock, A., Tagliaferri, G., Maccagni, D., & Garilli, B. 1989, in BL Lac Objects, ed. L. Maraschi, T. Maccacaro, & M.-H. Ulrich (Berlin: Springer-Verlag), 267
Bevington, T. R. 1969, Data Reduction and Error Analysis for the Physical Sciences (New York: McGraw-Hill)
Blandford, R., & Rees, M. J. 1978, Pittsburgh Conference on BL Lac Objects, ed. A. M. Wolfe (Pittsburgh: Univ. Pittsburgh Press), 328
Bregman, J. N. 1985, ApJ, 288, 32
———. 1990, A&A Rev., 2, 125
Eracleous, M., & Halpern, J. 1993, ApJ, 409, 584
Garilli, B., & Maccagni, D. 1990, A&A, 229, 88
George, I. M., Warwick, R. S., & Bromage, G. E. 1988a, MNRAS, 232, 793
George, I. M., Warwick, R. S., & McHardy, I. M. 1988b, MNRAS, 235, 787
Ghisellini, G., & Maraschi, L. 1989, ApJ, 340, 181
Ghisellini, G., Maraschi, L., & Treves, A. 1985, A&A, 146, 204
Ghisellini, G., Padovani, P., Celotti, A., & Maraschi, L. 1993, ApJ, 407, 65
Ghosh, K. K., & Soundararajaperumal, S. 1991, AJ, 102, 1298
Giommi, P., Barr, P., Garilli, B., Gioia, I. M., Maccacaro, T., Maccagni, D., & Schild, R. E. 1987, ApJ, 322, 662
Giommi, P., Barr, P., Garilli, B., Maccagni, D., & Pollack, A. M. T. 1990, ApJ, 356, 432
Giommi, P., et al. 1991, ApJ, 378, 77
Grandi, P., Tagliaferri, G., Giommi, P., Barr, P., & Palumbo, G. G. C. 1992, ApJS, 82, 93
Hartman, R. C. 1993, in Proc. 2d Compton Symp., in press
Hartman, R. C., et al. 1993, ApJ, 407, L41
Hunter, S. D., et al. 1993, A&A, 272, 59
Jones, T. W., O'Dell, S. L., & Stein, W. A. 1974, ApJ, 188, 353
Kii, T., et al. 1991, in Frontiers of X-Ray Astronomy, ed. Y. Tanaka & K. Koyama (Tokyo: Universal Academy Press), 577
Königl, A. 1981, ApJ, 243, 700
Lawson, A. J., Turner, M. J. L., Williams, O. R., Stewart, G. C., & Saxton, R. D. 1992, MNRAS, 259, 743
Ledden, J. E., & O'Dell, S. L. 1985, ApJ, 298, 630
Maccacaro, T., Gioia, I. M., Wolter, A., Zamorani, G., & Stocke, J. T. 1988, ApJ, 326, 680
Maccagni, D., Garilli, B., Schild, R., & Tarenghi, M. 1987, A&A, 178, 21
Madejski, G. M., & Schwartz, D. A. 1989, in BL Lac Objects, ed. L. Maraschi, T. Maccacaro, & M.-H. Ulrich (Berlin: Springer-Verlag), 267
Maraschi, L. 1992, in Variability of Blazars, ed. E. Valtaoja & M. Valtonen (Cambridge: Cambridge Univ. Press), 447
Maraschi, L., Ghisellini, G., Tanzi, E. D., & Treves, A. 1986, ApJ, 310, 325
Maraschi, L., & Maccagni, D. 1988, Mem. Soc. Astron. Ital., 59, 277
Marscher, A. P. 1980, ApJ, 235, 386
Melia, F., & Königl, A. 1989, ApJ, 340, 162
Ohashi, T. 1989, in BL Lac Objects, ed. L. Maraschi, T. Maccacaro, & M.-H. Ulrich (Berlin: Springer-Verlag), 296
Ohashi, T., Makishima, K., Inoue, H., Koyama, K., Makino, F., Turner, M. J. L., & Warwick, R. S. 1989, PASJ, 41, 709
Padovani, P. 1992, MNRAS, 257, 404
Padovani, P., & Urry, C. M. 1990, ApJ, 356, 75
Piccinotti, G., Mushotzky, R. F., Boldt, E. A., Holt, S. S., Marshall, F. E., Serlemitsos, P. J., & Shafer, R. A. 1982, ApJ, 253, 485
Remillard, R. A., Tuohy, I. R., Brissenden, R. J. V., Buckley, D. A. H., Schwartz, D. A., Feigelson, E. D., & Tapia, S. 1989, ApJ, 345, 140
Sambruna, R. M., Barr, P., Giommi, P., Maraschi, L., Tagliaferri, G., & Treves, A. 1994, ApJS, in press (Paper I)
Sambruna, R. M., Barr, P., Maraschi, L., Tagliaferri, G., & Treves, A. 1993, ApJ, 408, 452 (S93)
Schwartz, D. A., Doxsey, R. E., Griffiths, R. E. Johnston, M. D., & Schwartz, J. 1979, ApJ, 229, L53
Schwartz, D. A., & Ku, W. H.-M. 1983, ApJ, 266, 459
Sembay, S., Warwick, R. S., Urry, C. M., Sokoloski, J., George, I. M., Makino, F., Ohashi, T., & Tashiro, M. 1993, ApJ, 404, 112
Singh, K. P., Rao, A. R., & Vahia, M. N. 1990, ApJ, 365, 455
Staubert, R., Bazzano, A., Ubertini, P., Brunner, H., Collmar, W., & Kendziorra, E. 1986, A&A, 162, 16
Staubert, R., Brunner, H., & Worrall, D. M. 1986, ApJ, 310, 694
Stocke, J. T., Liebert, J., Schmidt, G., Gioia, I. M., Maccacaro, T., Schild, R. E., Maccagni, D., & Arp, H. C. 1985, ApJ, 298, 619
Stocke, J. T., Morris, S. L., Gioia, I., Maccacaro, T., Schild, R. E., & Wolter, A. 1990, ApJ, 348, 141
Stocke, J. T., Morris, S. L., Gioia, I., Maccacaro, T., Schild, R. E., Wolter, A., Fleming, T. A., & Henry, J. P. 1991, ApJS, 76, 813
Thompson, D. J., et al. 1993, ApJ, 410, 87
Treves, A., Belloni, T., Falomo, R., Fink, H., Maraschi, L., Sambruna, R. M., Tagliaferri, G., & Zimmermann, H. U. 1993, ApJ, 406, 447
Treves, A., et al. 1989, ApJ, 341, 733
Turner, T. J., & Pounds, K. A. 1989, MNRAS, 240, 833
Urry, C. M., & Mushotzky, R. F. 1982, ApJ, 253, 38
Wall, J. V., Danziger, I. J., Pettini, M., Warwick, R. S., & Wamsteker, W. 1986, MNRAS, 219, 23P
White, N. E., & Peacock, A. 1988, Mem. Soc. Astron. Ital., 59, 7
Worrall, D. M., & Wilkes, B. J. 1990, ApJ, 360, 396